Materials Science and Engineering B 177 (2012) 1628–1632

Contents lists available at SciVerse ScienceDirect

Materials Science and Engineering B

journal homepage: www.elsevier.com/locate/mseb

LBIC measurement optimization to detect laser annealing induced defects in Si

Yannick Larmande[a,*], Vanessa Vervisch[a], Philippe Delaporte[a], Gaëlle Coustillier[a], Thierry Sarnet[a], Marc Sentis[a], Hasnaa Etienne[b], Frank Torregrosa[b]

[a] LP3 Laboratory, UMR 7341 CNRS – Univ. de la Méditerranée, Campus de Luminy, Case 917, 13 288 Marseille Cedex 9, France
[b] Ion Beam Services, Rue Gaston Imbert Prolongée, 13 790 Peynier, France

ARTICLE INFO

Article history:
Received 23 March 2012
Received in revised form 20 June 2012
Accepted 15 August 2012
Available online 30 August 2012

Keywords:
Laser annealing
Plasma immersion ion implantation
Ultra shallow junctions
Light Beam Induced Current
Electrical measurements
Defects

ABSTRACT

Because of the short penetration depth of ultraviolet (UV) in semiconductor, the realization of UV sensors requires the reduction of the junction thickness. Excimer laser annealing (ELA) is a new annealing technical allowing to achieve a thin layer (<30 nm) heavily boron doped (R_{sq} < 350 Ω/sq) on n-type silicon substrate together with a good profile abruptness (<3 nm/dec).

The small size of the laser beam requires a scanning procedure for processing large surfaces. That could generate non-homogeneities resulting in defect growth. In order to investigate these phenomena, we developed a Light Beam Induced Current (LBIC) measurement set-up. LBIC analyses consist in the measurement of the photocurrent generated by a localized irradiation of the sample. The presence of defects in the irradiated zone leads to a local decrease of the photo-current. Moreover, thanks to different probe beams with wavelengths ranging from 193 nm to 800 nm, we can control the depth of photo-carriers generation. Thus, we are able to perform a 3D-localization of the defects which helps in understanding their origins.

We have developed and validated this detection method of defects generated in the ultra-thin junctions, down to thirty nanometers, with a spatial resolution of ten micrometers at the surface of the sample. First experimental results demonstrate that most of the defects are localized at the edge of the irradiated zone within the first ten nanometers from the surface.

1. Introduction

One of the challenges in microelectronics is the realization of USJ for the development of source/drain extension in CMOS. This step requires highly doped junctions with a limited diffusion. Moreover, the realization of sensors for short wavelength radiations such as UV and deep UV, strongly absorbed by silicon, also requires the use of USJ. These last years, the excimer laser annealing technique has been investigated [1–7] and has demonstrated its ability to achieve USJ. In a previous work [3,4], we have studied the realization of such junction by the association of plasma immersion ion implantation (PIII) technique, for doping a thin layer of silicon with low energy ions, and laser annealing for the activation of these ions in the silicon crystalline structure. We have demonstrated that well controlled laser irradiations with an ArF excimer source allow the activation of doping elements above their solubility limit in silicon and without further diffusion. 30 nm thick junctions have been realized with sheet resistance of 500 Ω/sq and abruptness of 2.5 nm/dec. However, laser annealing of surfaces larger than the beam size, typically less than 1 cm^2, requires a scanning procedure of the substrate with a controlled beam overlap. Such localized irradiations induce strong temperature gradient at the edge of the beam spot. We can then expect the generation of defects due to this non homogeneous annealing treatment of the surface. These defects will have a deleterious effect on the junction characteristics by increasing the leakage current. Moreover, the realization of high quality UV detector requires a uniform response of the detector over the whole surface. For the development of this technology, it is then of prime importance to characterize these defects, in order to understand their formation mechanisms and to optimize the annealing protocol in order to avoid them. This work addresses the first step of this study: the detection and localization of the defects in the annealed volume.

Many techniques have been developed to characterize the junction properties, such as sheet resistance and leakage current, with high spatial resolution. We can mention the Junction Photo-Voltage measurement under modulated irradiation [8], minority carrier lifetime measurements [9] and Light Beam Induced Current (LBIC) analyses [10–13]. This last optical scanning technique is based on the measurement of the current generated in the junction when a local irradiation of its surface is performed with a probe beam. When defects are in the volume of light absorption, they will act

* Corresponding author. Tel.: +33 4 91 82 92 82; fax: +33 4 91 82 92 89.
E-mail address: larmande@lp3.univ-mrs.fr (Y. Larmande).

0921-5107/$ – see front matter © 2012 Elsevier B.V. All rights reserved.
http://dx.doi.org/10.1016/j.mseb.2012.08.018

Table 1
Optical properties of silicon for the different sources used [14].

Sources	Wavelength λ (nm)	Photon energy E_γ (eV)	Penetration depth α^{-1} (nm)	Reflective coefficient R (%)
Arf laser	193	6.44	5.6	68.8
Xe lamp	400	3.11	82	48.6
HeNe laser	633	1.96	2290	35.1
Xe lamp	800	1.55	7960	33.1

as recombination centers for minority carriers, and the collected current will be reduced. Then, LBIC appears to be a very efficient tool for the localization of the defects in the junction, with a high spatial resolution.

In this study, we developed and optimized the LBIC technique (presented in Fig. 1) for the detection of crystallization defects induced by localized laser annealing of silicon substrate. In order to investigate not only the 2D localization of these defects, but also the depth at which they are generated, we used four probe light beams with different wavelengths corresponding to different absorption lengths below the surface.

2. Experiment

The samples used in this study are n-type silicon wafers with a resistivity of 500 Ω cm. Boron implantation is performed with PULSION®, a plasma immersion ion implanter patented by Ion Beam Services (IBS) company. An acceleration voltage of 1 kV allows us to introduce a saturation dose of 6×10^{15} at./cm^2. After implantation, the samples are annealed with an ArF excimer laser (λ = 193 nm, 15 ns pulse duration). The uniformity of the laser energy density on the silicon surface is one of the key parameters to guarantee a uniform junction. The uniformity of the beam was achieved with an homogenizer based on Diffractive Optics Elements (DOEs) from SILIOS company. The spatial distribution of the energy, at the surface of silicon wafer, obtained with this set-up is presented in Fig. 2. In this work, the energy density was fixed at 700 mJ/cm^2, leading to the realization of an USJ with a sheet resistance of 350 Ω/sq, and a junction depth of 30 nm.

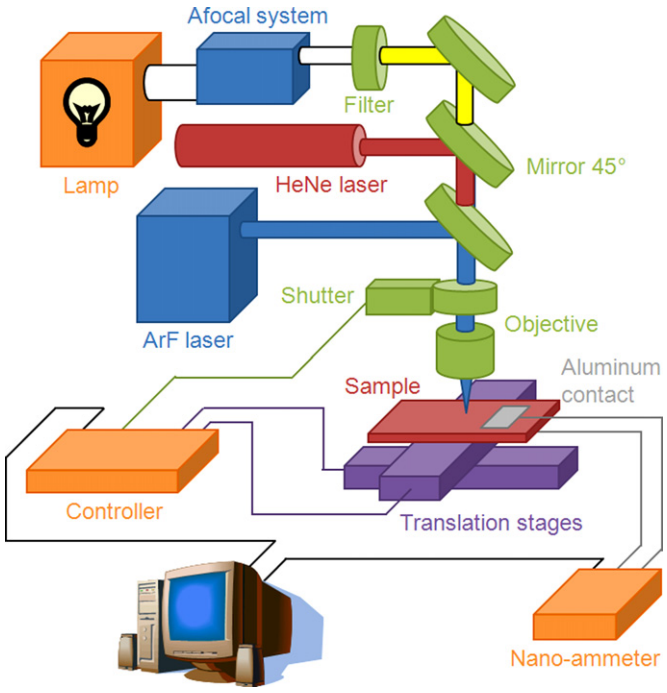

Fig. 1. Schematic of the LBIC set-up.

After annealing, an 500 nm thick aluminum strip of is deposited by thermal evaporation through a mask on the edge of the activated zone in order to collect electrons.

The scheme of the LBIC setup is represented in Fig. 1. Four light sources have been used to investigate the defects location as a function of the depth. A white lamp (Collimated Xenon Arc Lamp Source made by Oriel Instruments – 150 W) was used with two filters centered at 400 nm and 800 nm, with a bandwidth of ±40 nm. A HeNe laser was used to probe the sample at 633 nm. At last, a 200 Hz, 10 mJ, ArF excimer laser, was used to perform analyses at 193 nm, using energy densities lower than the melting threshold. The optical properties of silicon at these wavelengths are summarized in Table 1. Especially, the evolution of the optical absorption lengths as a function of the wavelength shows why these sources allow us to determine the photo-current generated at different depths. The beam light, which is diaphragmed with a hardmask to the output of the source, is focused by means of a reflective objective, and the spot diameter at the sample surface is lower than 10 μm when the lasers are used and around 20 μm with the lamp. A mechanical shutter is used to transform the continuous beams (HeNe laser and white light source) in pulsed beams. When using the ArF laser as the probe source, sequences of 7 shots at 200 Hz were used at the same location to increase the amount of photo-current, while keeping the energy density per pulse smaller than the melting threshold of the substrate.

Two translation stages, with a resolution of 1 μm, allow the computer-controlled motion of the sample perpendicularly to the probe beam propagation axis. An area up to 25 mm × 25 mm, can be analyzed with this set-up. The photo-current is collected and amplified by a low-noise current preamplifier (Stanford Model SR570), and then a multimeter (Fluke 8846A) measures the amplified current during 50 ms. The sample analysis is fully automatic. The computer controls and synchronizes the translation stages, the triggering of the ArF laser or the shutter, and the acquisition of the photo-current values. All the measurements are performed in air at room temperature.

3. Results

First, we performed laser annealing with four laser spots on the same area and we deposited the aluminum contact with a small overlap on the irradiated zone in order to collect the photocurrent. Then, we realized LBIC measurements with the HeNe laser source.

Fig. 2 compares the energy profile of the annealing laser beam analyzed by a CCD camera (Gentec Beamage-CCD23 using an UV converter) and the map of the photocurrent collected during the LIBC analysis. One can observe that in both directions the LBIC profiles are sharper than the energy profiles of the laser beam. Indeed, the annealed region is limited by the melting of silicon. The dopants were moved in substitutional sites only if the silicon has been melted. When the local laser fluence decreases below the melting threshold, there is no activation and therefore no generation of photocurrent when this zone is probed. This result shows that, due to the short pulse duration, there is no significant thermal diffusion and the activated surface is equal to the irradiated zone with fluence higher than melting threshold. Moreover, irradiation at lower fluence at the edges of the laser spot does not lead

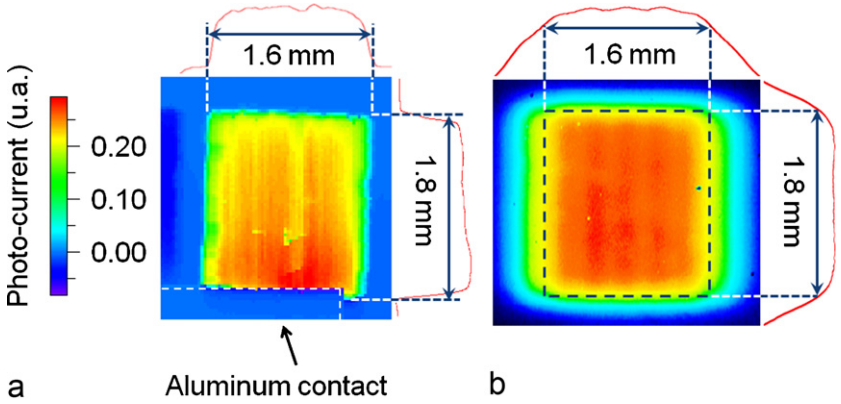

Fig. 2. (a) Photo-current measured on the area annealed by four laser impacts at the same place and (b) measurement of the laser beam spatial distribution energy.

to activation in sub-melt regime. We note that, although the lower part of the photo-current map is more intense because the collection electrode is closer, the measurement gives a quite uniform response over the annealed zone, and does not reveal the presence of defects.

Then, the defects generated by the edges of the laser beam have been investigated by means of LBIC analysis of five laser impacts separated by a distance of 0.35 mm. This length corresponds to an overlap of 75% between two successive impacts. We perform 1D photo-current measurements in the direction of the annealing laser motion, and parallel to the metallic contact to prevent any variation of the response due different distances between irradiated zone (carrier generation) and collection electrode. The four different probe sources have been used to generate carriers at different depth as a function of the probe wavelength. Fig. 3 schematizes the laser annealing and LBIC analysis protocols used for this set of experiments. We averaged the signal on five consecutive measurements to increase the signal-to-noise ratio.

Fig. 4 presents the photo-current intensity as a function of the position along the line on the annealed region (see Fig. 3), for different probe beam wavelengths. Measurements performed with sources emitting at 633 nm and 800 nm lead to flat and uniform profiles, while the profiles recorded with lower wavelength probe light (400 nm and 193 nm) exhibit significant fluctuations. At 400 nm, the edges of the annealed zone present an increase of the photo-current, probably due to an edge effect of the junction, but we cannot provide any clear explanation of this effect. However, no significant signal variations can be observed in the central part of the analyzed zone. At last, the photocurrent curve recorded when the sample is probed with a UV light at 193 nm clearly exhibits four negative peaks. They correspond to a decrease of the photocurrent in four specific zones. These peaks present similar amplitude and width and they are separated each other by 0.35 mm, which is exactly the distance between each annealing impact. Then, we can assume that probing with the ArF laser allows us the detection of annealing defects in silicon. The average value of the photocurrent signal increases at the right hand side of the curve, between 2.5 mm and 3.5 mm, and that could be related to a shorter distance between the probed point and the collection electrode. Indeed, when the scan is not achieved strictly parallel to the aluminum contact, the amount of photo-carriers collected varies with the distance. It increases when the distance decreases because the probability of recombination also decreases.

The reason why these defects can only be observed with a UV probe beam emitting at 193 nm is related to the evolution of the penetration depth of the incident light in the silicon as a function of the wavelength. Table 1 summarizes the optical properties of silicon for the four wavelengths used as LBIC source. The penetration depths at 633 nm or 800 nm are much higher (>2 μm) than the depth of the analyzed junctions. Then, most of the photo-carriers are generated beyond the junction, in a region which has not been implanted and annealed, and therefore without defects. When a probe beam of 400 nm is used, the absorption thickness (80 nm) is two times higher than the junction depth. The proportion of photo-carriers generated beyond the junction is then very high. These carriers will not meet defects and will contribute, like the 633 nm

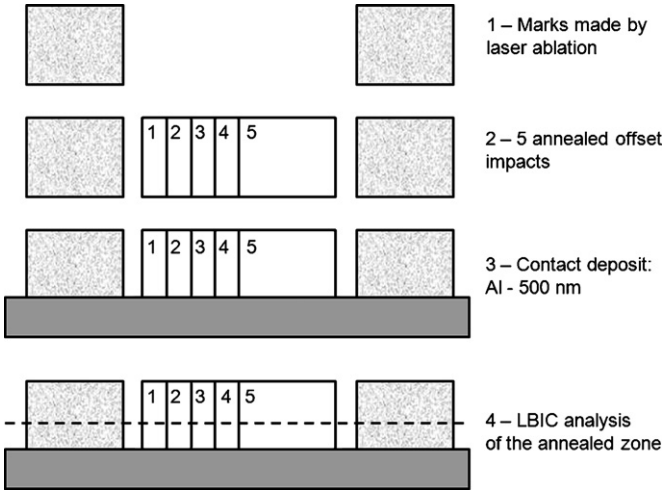

Fig. 3. Schematic of samples realization and analysis.

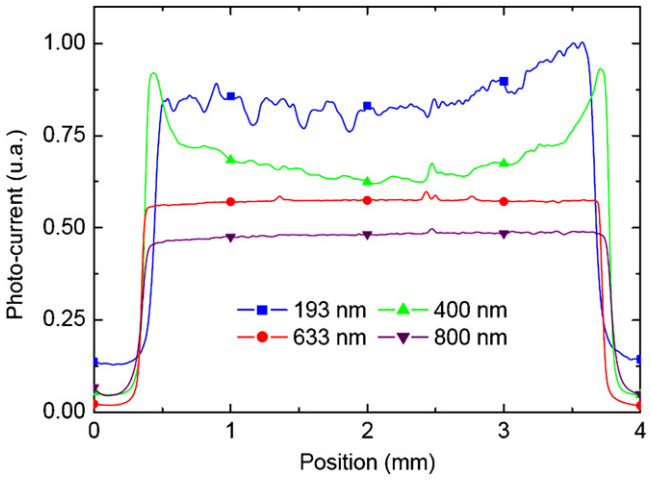

Fig. 4. Photo-current measured as a function of the position on the annealed region, for different measurement sources.

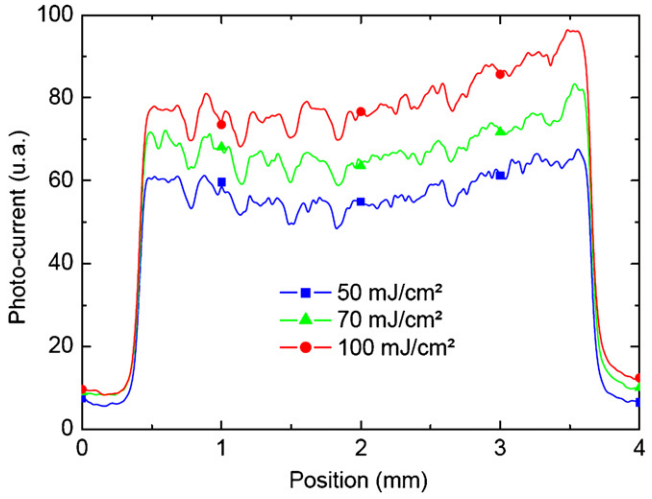

Fig. 5. Photo-current measured as a function of the position on the annealed region, for different ArF energy densities.

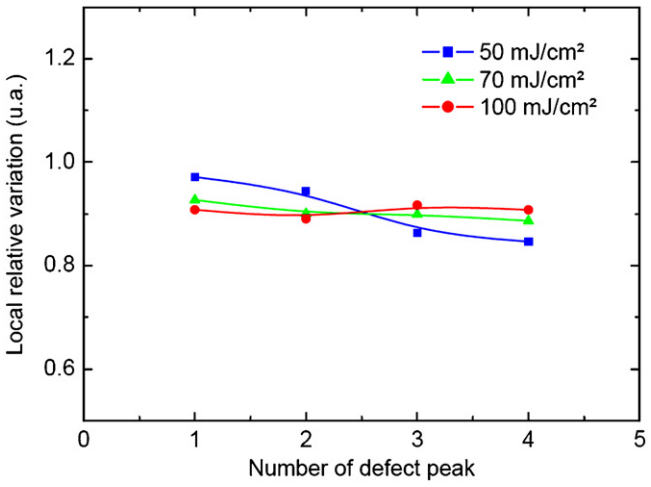

Fig. 6. Variation of relative intensity of the "defects" peaks for different energy densities.

or 800 nm source, to hide the recombination due to defects within the junction. Finally, the use of an UV light, such as the ArF laser, as a LBIC probe source leads to an absorption of the photons energy within a depth lower than 10 nm. In this situation, the generation of all the photo-carriers takes place within the junction. The recombination proportion is then greater than for irradiation at longer wavelengths and that significantly affects the photocurrent signal.

The ratio of the photo-carriers generated within the junction by the absorption of the laser energy of the probe beam can be estimated from the Beer–Lambert law. It describes the laser intensity as a function of the penetration depth (z) inside the silicon substrate.

$$I(z) = I_0(1-R)e^{-\alpha z} \quad (1)$$

where I_0 represents the incident laser intensity at the substrate surface ($z=0$), R the reflectivity of the surface and α the absorption coefficient. These two parameters, R and α, are wavelength dependent. Then, we can estimate the number, n, of photons absorbed inside the volume of the junction:

$$n(X_j) = I(0) - I(X_j) = I_0(1-R)(1-e^{-\alpha X_j}) \quad (2)$$

where X_j is the junction thickness. The relative amount, RA, of photo-carriers generated inside the junction can be deduced from Eq. (2):

$$RA = \frac{n(X_j)}{n(z\to\infty)} = (1-e^{-\alpha X_j}) \quad (3)$$

From Eq. (3) and the data provided in Table 1, we can approximate the relative amount of photo-carriers generated inside the junction for the different probe wavelengths used in this study. In particular, for a junction of 30 nm, the proportion of carriers generated inside the junction is 30% at 400 nm and 99% at 193 nm. This strong difference can explain that the defects are only revealed when an ArF probe beam is used.

The influence of probe beam intensity on photo-current signal has been investigated in order to optimize the sensitivity of this LBIC technique and then to improve the detection of the defects. Then, we varied the energy density of the ArF probe beam between 50 mJ/cm^2 and 100 mJ/cm^2. Fig. 5 presents the photo-current curves recorded when probing the same line of the sample with 3 different fluences. We can observe that an increase of the energy density of the probe beam does not affect the curve profile, but induces an increase of the collected photo-current. However, this increase is not proportional to the incident intensity. It seems limited by the ability of photodiode to convert photons to electrons when a large amount of photons is absorbed. This saturation effect is certainly enhanced by the short pulse duration of the ArF probe beam.

Fig. 6 represents the relative intensities of the four negative peaks, representative of the defects generated in the junction, for the three curves of Fig. 5. These measurements correspond to the ratio between the minimum value of the peak and an average value calculated locally around the peak. There are no significant variations of the relative intensity of the peaks when the probe intensity is varied. These results lead to the conclusion that the energy density does not alter the ability of LBIC analysis to observe the defects.

However, an energy density of 100 mJ/cm^2 represents a significant proportion of the energy density used during the activation process (700 mJ/cm^2), with an ArF laser. In order to guarantee that this probe beam does not modify the substrate properties when such a high energy density is used, several successive measurements have been performed on the same region. All the photo-current curves recorded during this study were similar, and that allows us to conclude that probing the sample with an energy density of 100 mJ/cm^2 does not induce any significant modification of the sample properties.

In order to observe the whole annealed area, a mapping of this region has been performed by moving the sample in both directions (X and Y) under an ArF probe beam. Fig. 7 presents the photocurrent map of the surface analyzed with this LBIC method. On the left hand side of the picture, we can observe four dark vertical lines which correspond to the left edge of the activation laser impacts. We can assume that the defects are generated at both edges of the beam, but the defects created by the right hand side of the beam are not visible. Indeed, the sample was moved from the right to the left when annealed, and each new laser irradiation induces the melting of the

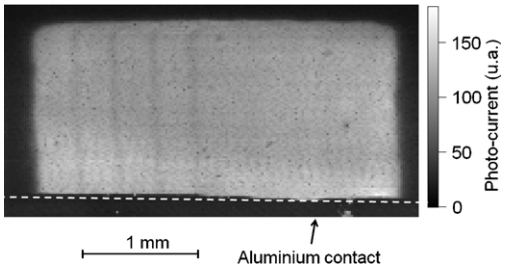

Fig. 7. LBIC mapping of 5 laser annealing spots separated by 0.35 mm. The probe beam was an ArF laser (193 nm).

zone and then of the edge defects previously generated in this area by the previous shots. Fig. 7 demonstrates clearly the ability of LBIC method, with an ArF laser as probe source, to provide a complete photo-current mapping of a surface, and to reveal defects inside the junction that cannot be detected with other optical techniques.

4. Conclusion

The LBIC analysis method has been improved to perform the observation of defects generated in ultra-shallow junctions by the laser activation process. Thanks to the high absorption coefficient of silicon at 193 nm, the use of an ArF laser as probe source increases the sensitivity of the method for the detection of defects in the first nanometers of the sample. This deep UV LBIC analysis appears as a unique characterization tool for the observation of a localized concentration of defects, inside a P/N junction. This study has demonstrated that the defects generated by the laser annealing process are localized at the edge of the laser beam. Moreover, we observe that these defects can be corrected by a single laser impact leading to the melting of the irradiated area. Thanks to these improvements of the LBIC technique, the study of the impact of the beam profile on the generation of defects is now possible.

Acknowledgements

This work has been carried out in the framework of the ALDIP project, supported by Conseil Général 13, PACA region and DGE.

References

[1] A. Florakis, D. Tsoukalas, I. Zergioti, K. Giannakopoulos, P. Dimitrakis, D.G. Papazoglou, G. Bennassayag, H. Bourdon, A. Halimaoui, Nuclear Instruments and Methods in Physics Research B253 (2006) 13–17.
[2] F. Torregrosa, C. Laviron, F. Milesi, M. Hernandez, H. Faïk, J. Venturini, Nuclear Instruments and Methods in Physics Research B237 (2005) 18–24.
[3] V. Vanessa, Y. Larmande, Ph. Delaporte, T. Sarnet, M. Sentis, H. Etienne, F. Torregrosa, F. Cristiano, P.F. Fazzini, Applied Surface Science 255 (2009) 5647–5650.
[4] V. Vervisch, H. Etienne, F. Torregrosa, L. Roux, L. Ottaviani, M. Pasquinelli, T. Sarnet, P. Delaporte, Journal of Vacuum Science and Technology B26 (2008) 286.
[5] J. Venturini, M. Hernandez, G. Kerrien, C. Laviron, D. Camel, J.L. Santailler, T. Sarnet, J. Boulmer, Thin Solid Films 453–454 (2004) 145–149.
[6] G. Fortunato, L. Mariucci, M. Stanizzi, V. Privitera, S. Whelan, C. Spinella, G. Mannino, M. Italia, C. Bongiorno, A. Mittiga, Nuclear Instruments Methods in Physics Research B186 (2002) 401–408.
[7] T. Sarnet, G. Kerrien, N. Yaakoubi, A. Bosseboeuf, E. Dufour-Gergam, D. Débarre, J. Boulmer, K. Kakushima, C. Laviron, M. Hernandez, J. Venturini, T. Bourouina, Applied Surface Science 247 (2005) 537–544.
[8] V.N. Faifer, M.L. Current, T. Nguyen, T.M.H. Wong, V.V. Souchkov, Materials Research Science – Symposium C, Proceedings 810C (2004), 11.9.
[9] L. Ottaviani, O. Palais, D. Barakel, M. Pasquinelli, Materials Science Forum 615–617 (2009) 295–298.
[10] I. Périchaud, J.J. Simon, S. Martinuzzi, Materials Science and Engineering B42 (1996) 265–269.
[11] N.M. Thantsha, E.Q.B. Macabebe, F.J. Vorster, E.E. van Dyk, Physica B404 (2009) 4445–4448.
[12] V. Sirotkin, S. Zaitsev, E. Yakimov, Materials Science and Engineering B 91–92 (2002) 260–263.
[13] P. Vorasayan, T.R. Betts, A.N. Tiwari, R. Gottschalg, Solar Energy Materials and Solar Cells 93 (2009) 917–921.
[14] Handbook of Chemistry and Physics, 85th ed., CRC Press, 2004–2005, 12–150.